VERSITA

Central European Journal of Physics
DOI: 10.2478/s11534-006-0028-8
Research article
CEJP 4(4) 2006 481–493

Atomic simulation of the vacancies in BCC metals with MAEAM

Jian-Min Zhang[1*], Yan-Ni Wen[1], Ke-Wei Xu[2]

[1] *College of Physics and Information Technology, Shaanxi Normal University, Xian 710062, Shaanxi, PR China*

[2] *State Key Laboratory for Mechanical Behavior of Materials, Xian Jiaotong University, Xian 710049, Shaanxi, PR China*

Received 13 December 2005; accepted 5 June 2006

Abstract: The formation energy of the mono-vacancy and both the formation energy and binding energy of the di- and tri-vacancy in BCC alkali metals and transition metals have been calculated by using the modified analytical embedded-atom method (MAEAM). The formation energy of each type of configuration of the vacancies in the alkali metals is much lower than that in the transition metals. From minimum of the formation energy or maximum of the binding energy, the favorable configuration of the di-vacancy and tri-vacancy respectively is the first-nearest-neighbor (FN) or second-nearest-neighbor (SN) di-vacancy and the [112] tri-vacancy constructed by two first- and one second-nearest-neighbor vacancies. It is indicated that there is a concentration tendency for vacancies in BCC metals.

Keywords: Vacancy, modified analytical embedded-atom method (MAEAM), BCC metals
PACS (2006): 30; 31.15.Ct; 32.80.Ys; 34.10.+x; 36.40.-c

1 Introduction

The configuration and concentration of vacancies that exist in metals affect directly the physical, chemical and mechanical properties of the metals [1]. The migration of vacancies or interstitials, as is well known, is the dominant mechanism of atom transport or diffusion in processes like solid phase transformation, crack formation and expanding and the other defects (including dislocation and interface) migration [2]. Vacancies also play an

* E-mail: jianm_zhang@yahoo.com

important role for surface morphology [3]. So, a detailed knowledge of the configuration and energy of vacancies is very important for understanding many phenomena associated with vacancies. Many indirect experimental methods, such as by measurements of heat capacity (special heat) [4], electrical resistivity [5], differential-dilatometer (thermal expansion not caused by the lattice but by increased number of vacancies) [6] and positron annihilation spectrum [7], have been used to measure the vacancy formation energy. A theoretical calculation or simulation is a useful supplement method.

In this paper, the formation energy of the mono-vacancy and both the formation energy and binding energy of three-type configurations of the di-vacancy and eight-type configurations of the tri-vacancy in body-central cubic (BCC) alkali metals and transition metals have been calculated by using the modified analytical embedded atom method (MAEAM). The MAEAM is an extension to the analytical embedded atom method (AEAM) [8–10] developed by Johnson and his coworkers by adding a modified term to describe the energy change due to the non-spherical distribution of electrons and deviation from the linear superposition of atomic electronic density.

2 MAEAM

In the MAEAM, the total energy of a system E_t is expressed as [11, 12]

$$E_t = \sum_i F(\rho_i) + \frac{1}{2}\sum_i \sum_{j(\neq i)} \phi(r_{ij}) + \sum_i M(P_i) \tag{1}$$

$$\rho_i = \sum_{j(\neq i)} f(r_{ij}) \tag{2}$$

$$P_i = \sum_{j(\neq i)} f^2(r_{ij}) \tag{3}$$

where $F(\rho_i)$ is the energy to embed an atom in site i with electron density ρ_i, which is given by a linear superposition of the spherical averaged atomic electron density of other atoms $f(r_{ij})$, r_{ij} is the separation distance of atom j from atom i, $\phi(r_{ij})$ is the interaction potential between atoms i and j, and $M(P_i)$ is the modified term that describes the energy change due to the non-spherical distribution of electron P_i and deviation from the linear superposition of atomic electronic density. The embedding function $F(\rho_i)$, pair potential $\phi(r_{ij})$, modified term $M(P_i)$ and atomic electron density $f(r_{ij})$ are taken as following forms [13]

$$F(\rho_i) = -F_0\left[1 - n\ln(\rho_i/\rho_e)\right](\rho_i/\rho_e)^n \tag{4}$$

$$\phi(r_{ij}) = k_0 + k_1(r_{ij}/r_{1e})^2 + k_2(r_{ij}/r_{1e})^4 + k_3(r_{1e}/r_{ij})^{12} \tag{5}$$

$$M(P_i) = \alpha(P/P_e - 1)^2 \exp[-(P/P_e - 1)^2] \tag{6}$$

$$f(r_{ij}) = f_e(r_{1e}/r_{ij})^6 \tag{7}$$

where the subscript e indicates equilibrium state and r_{1e} is the first-nearest-neighbor distance at equilibrium. The cut-off distance of interaction potential for BCC metal r_c,

where the pair potential and its slope are zero, lies between the second- and third-nearest-neighbor distance. That is

$$r_c = r_{2e} + 0.75(r_{3e} - r_{2e}) \tag{8}$$

According to the principle that the energy vs. separation distance curve fits the Rose equation [14] as far as possible and the ref. [12, 15], eight model parameters, F_0, n, α, f_e, k_i $(i = 0 \sim 3)$ can be calculated with the following equations from the lattice constant a, the cohesive energy E_c, mono-vacancy formation energy E_{1f} and the elastic constants C_{11}, C_{12} and C_{44} of the BCC metal considered.

$$F_0 = E_c - E_{1f} \tag{9}$$

$$n = \sqrt{\Omega(C_{11} + 2C_{12})(C_{11} - C_{12})/(216E_{1f}C_{44})} \tag{10}$$

$$\alpha = \Omega(C_{12} - C_{44})/5126.4 - n^2F_0/8 \tag{11}$$

$$f_e = [(E_c - E_{1f})/\Omega]^{3/5} \tag{12}$$

$$k_0 = -E_{1f}/7 - \Omega(51519C_{44} + 57111C_{12} - 57111C_{11})/75582360 \tag{13}$$

$$k_1 = \Omega(33327C_{44} + 52563C_{12} - 52563C_{11})/43189920 \tag{14}$$

$$k_2 = \Omega(147456C_{11} - 147456C_{12} - 59049C_{44})/302329440 \tag{15}$$

$$k_3 = 1536\Omega(4C_{44} - C_{11} + C_{12})/66134565 \tag{16}$$

where $\Omega = a^3/2$ is the atomic volume in BCC metals.

For convenience, the input physical parameters and calculated model parameters for BCC metals are listed in Table 1 and Table 2 respectively.

Table 1 Input parameters for BCC metals [16–18].

Metals	a/nm	E_c/eV	E_{1f}/eV	C_{11}/eV·nm^{-3}	C_{12}/eV·nm^{-3}	C_{44}/eV·nm^{-3}
Li	0.35093	1.63	0.48	84	71	55
Na	0.42096	1.113	0.34	46	39	26
K	0.5321	0.934	0.34	28	23	16
Rb	0.5703	0.852	0.341	18	15	10
Cs	0.6141	0.804	0.322	15	9	13
Fe	0.28664	4.28	1.79	1440	840	730
W	0.31650	8.90	3.95	3230	1270	980
Mo	0.31468	6.82	3.10	2870	1050	690
Cr	0.28846	4.10	1.60	2160	410	620
Ta	0.33026	8.10	2.95	1640	970	520
Nb	0.33007	7.57	2.75	1530	820	180
V	0.30282	5.31	2.10	1440	750	270

Table 2 Calculated model parameters for BCC metals.

Metals	F_0/eV	n	α	f_e	k_0/eV	k_1/eV	k_2/eV	k_3/eV
Li	1.1500	0.1055	-0.0015	0.1720	-0.0694	0.0006	-0.0001	0.0001
Na	0.7730	0.1302	-0.0015	0.0977	-0.0492	0.0004	-0.0001	0.0001
K	0.5940	0.1540	-0.0017	0.0547	-0.0494	0.0005	-0.0001	0.0001
Rb	0.5110	0.1347	-0.0011	0.0441	-0.0493	0.0004	-0.0001	0.0001
Cs	0.4820	0.1592	-0.0016	0.0373	-0.0470	0.0003	0.0001	0.0001
Fe	2.4900	0.2795	-0.0241	0.3937	-0.2610	-0.0020	0.0018	0.0006
W	4.9500	0.4630	-0.1318	0.4974	-0.5725	-0.0121	0.0121	0.0007
Mo	3.7200	0.5523	-0.1407	0.4234	-0.4480	-0.0262	0.0117	0.0003
Cr	2.5000	0.5405	-0.0918	0.3901	-0.2321	-0.0198	0.0088	0.0002
Ta	5.1500	0.3611	-0.0824	0.4718	-0.4269	-0.0075	0.0041	0.0006
Nb	4.8200	0.6152	-0.2258	0.4539	-0.3941	-0.0130	0.0056	0.0001
V	3.2100	0.4796	-0.0910	0.4153	-0.3018	-0.0088	0.0039	0.0001

3 Energy calculation and discussion

3.1 Mono-vacancy

Mono-vacancy can be formed by removing one atom from the central site of a crystal with N atoms and the formation energy of mono-vacancy E_{1f} can be calculated by

$$E_{1f} = E_t^{N-1} - \frac{E_t^N}{N}(N-1) \tag{17}$$

where E_t^{N-1} and E_t^N is the total energy of the crystal with and without mono-vacancy respectively. In order to avoid the influence of the boundary, we assume the inner computational cell of the crystal is surrounded by a mantle of atoms fixed at their perfect lattice positions. The computational cell is a $10a \times 10a \times 10a$ crystal, where a is the lattice constant. The mantle ensures that each atom in the computational cell has a complete set of neighbors with the range of the interatomic potential used.

The energies of the atoms near the vacancies were affected by the vacancies, therefore, the computational cell should include all the affected atoms. The fewer the number of the vacancies, the fewer the number of atoms there are in the computational cell. But for consistency, we only choose the same $10a \times 10a \times 10a$ computational cell in the whole paper. Of course, if there are many vacancies considered, the computational cell should be changed.

Calculated formation energies of mono-vacancy are listed in Table 3 together with the available experimental values for BCC alkali metals [18] and transition metals [19]. It can be seen that the calculated results are in good agreement with the available experimental values. The highest mono-vacancy formation energy corresponds to transition metal W, and the formation energy of the mono-vacancy in alkali metals is much lower than that in the transition metals. As is well known and obvious, the value of the mono-vacancy

formation energy of each metal is related directly to its cohesive energy E_c, that is, the higher the cohesive energy is, the higher the mono-vacancy formation energy is.

Table 3 Formation energy (eV) of the mono-vacancy in BCC metals.

Metals	Li	Na	K	Rb	Cs	Fe
Cal.	0.4809	0.3408	0.3413	0.3420	0.3249	1.8173
Exp.	0.482	0.342	0.348			1.8
Metals	W	Mo	Cr	Ta	Nb	V
Cal.	4.0632	3.1978	1.6759	2.9857	2.7509	2.1215
Exp.	3.6	3.2	2.1	3.1	2.7	2.1

3.2 Di-vacancy

A similar calculation is also conducted for the di-vacancy. Three-type configurations of the di-vacancy, the first-, second- and third-nearest-neighbor di-vacancy (simply noted as FN, SN and TN respectively), are considered. As shown in Fig. 1. they are introduced by removing two atoms from sites (0,0,0) and (a/2, a/2, a/2) (a), (0,0,0), and (a,0,0) (b), and (0,0,0) and (a,0,a) (c) respectively in the inner computational cell.

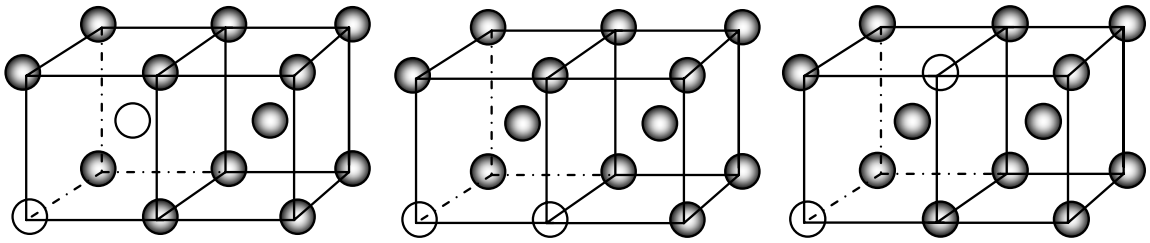

(a) FN (b) SN (c) TN

Fig. 1 Three-type configurations of the di-vacancy: (a) the first-nearest-neighbor (FN), (b) the second-nearest-neighbor (SN), (c) the third-nearest-neighbor (TN).

The formation and binding energy of the di-vacancy can be calculated by

$$E_{2f} = E_t^{N-2} - \frac{E_t^N}{N}(N-2) \tag{18}$$

$$E_{2b} = 2E_{1f} - E_{2f} \tag{19}$$

where E_t^{N-2} and E_t^N is the total energy of the crystal with and without di-vacancy respectively. The calculated results are listed in Table 4 for three-type configurations of the di-vacancy in BCC metals. It can be seen that, similar to the mono-vacancy, the formation energy of each type of configuration of the di-vacancy in alkali metals is much lower than that in transition metals. For each metal, the formation energy increases

with FN, SN and TN di-vacancy successively, that is $E_{2f}^{FN} < E_{2f}^{SN} < E_{2f}^{TN}$, however, the binding energy decreases with FN, SN and TN successively, that is $E_{2b}^{FN} > E_{2b}^{SN} > E_{2b}^{TN}$. With nearly the same formation and binding energies for the FN and the SN di-vacancies, this shows that these two-type configurations of the di-vacancy exist simultaneously in BCC metals. The negative binding energy corresponding to the TN di-vacancy indicates the TN di-vacancy is difficult to form in BCC metals.

Table 4 Calculated formation and binding energy (eV) of three-type configurations of the di-vacancy in BCC metals.

Metals	E_{2f}^{FN}	E_{2b}^{FN}	E_{2f}^{SN}	E_{2b}^{SN}	E_{2f}^{TN}	E_{2b}^{TN}
Li	0.8934	0.0684	0.8935	0.0683	0.9621	-0.0003
Na	0.6333	0.0483	0.6333	0.0483	0.6819	-0.0003
K	0.6342	0.0484	0.6344	0.0482	0.6829	-0.0003
Rb	0.6354	0.0486	0.6355	0.0485	0.6842	-0.0002
Cs	0.6037	0.0461	0.6038	0.0460	0.6500	-0.0002
Fe	3.3795	0.2551	3.3807	0.2539	3.6381	-0.0035
W	7.5705	0.5559	7.5756	0.5508	8.1450	-0.0186
Mo	5.9650	0.4306	5.9701	0.4255	6.4153	-0.0197
Cr	3.1293	0.2225	3.1325	0.2193	3.3645	-0.0127
Ta	5.5604	0.4110	5.5639	0.4075	5.9832	-0.0118
Nb	5.1510	0.3508	5.1587	0.3431	5.5332	-0.0314
V	3.9571	0.2859	3.9606	0.2824	4.2559	-0.0129

3.3 Tri-vacancy

Eight-type configurations of the tri-vacancy are considered (as shown in Fig. 2): (a) two first- and one second-nearest-neighbor noted as [112] for simplicity; (b) two first- and one third-nearest-neighbor [113]; (c) two first- and one fifth-nearest-neighbor [115]; (d) one first-, one second- and one forth-nearest-neighbor [124]; (e) two second- and one third-nearest-neighbor [223]; (f) two second- and one sixth-nearest-neighbor [226]; (g) one second-, one third- and one fifth-nearest-neighbor [235]; and (h) three third-nearest-neighbor [333].

Similar to the di-vacancy, the formation and binding energy of the tri-vacancy can be calculated by

$$E_{3f} = E_t^{N-3} - \frac{E_t^N}{N}(N-3) \tag{20}$$

$$E_{3b} = 3E_{1f} - E_{3f} \tag{21}$$

The calculated values of the formation energy and binding energy are listed in Table 5 and Table 6 for eight-type configurations of the tri-vacancy in BCC metals.

The formation energies of eight-type configurations of the tri-vacancy in BCC alkali metals and transition metals are illustrated in Fig. 3 and Fig. 4 respectively. Similar

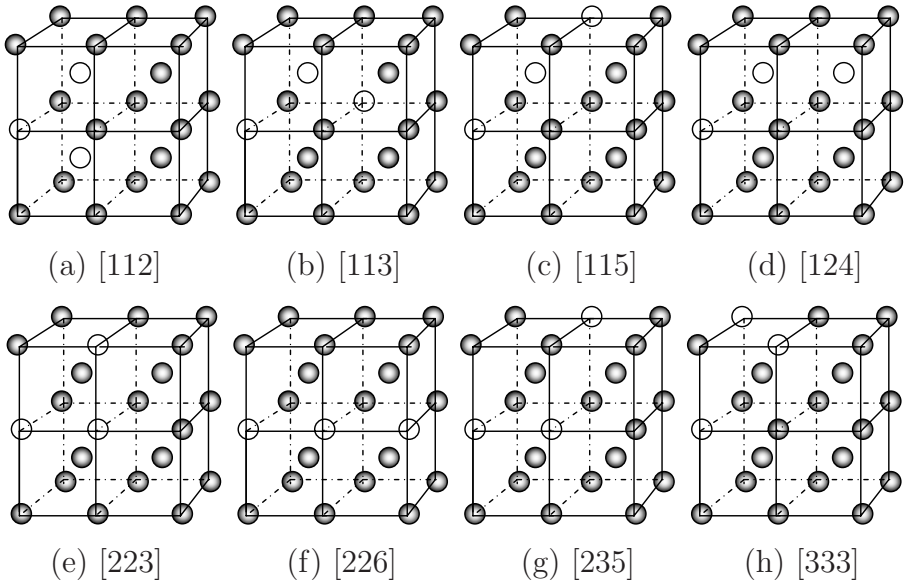

Fig. 2 Eight-type configurations of the tri-vacancy: (a) two first- and one second-nearest-neighbor [112]; (b) two first- and one third-nearest-neighbor [113]; (c) two first- and one fifth-nearest-neighbor [115]; (d) one first-, one second- and one forth-nearest-neighbor [124]; (e) two second- and one third-nearest-neighbor [223]; (f) two second- and one sixth-nearest-neighbor [226]; (g) one second-, one third- and one fifth-nearest-neighbor [235]; and (h) three third-nearest-neighbor [333].

Table 5 Formation energy (eV) of eight-type configurations of the tri-vacancy in BCC metals.

Metals	$E_{3f}^{[112]}$	$E_{3f}^{[113]}$	$E_{3f}^{[115]}$	$E_{3f}^{[124]}$	$E_{3f}^{[223]}$	$E_{3f}^{[226]}$	$E_{3f}^{[235]}$	$E_{3f}^{[333]}$
Li	1.2375	1.3061	1.3060	1.3061	1.3065	1.3062	1.3749	1.4435
Na	0.8773	0.9259	0.9257	0.9259	0.9262	0.9259	0.9746	1.0232
K	0.8787	0.9273	0.9272	0.92274	0.9277	0.9274	0.9761	1.0249
Rb	0.8801	0.9289	0.9288	0.9289	0.9292	0.9290	0.9778	1.0266
Cs	0.8362	0.8826	0.8824	0.8826	0.8829	0.8826	0.9290	0.9754
Fe	4.6855	4.9439	4.9419	4.9441	4.9484	4.9440	5.2037	5.4630
W	10.5148	11.0897	11.0792	11.0897	11.1108	11.0881	11.6689	12.2484
Mo	8.2936	8.7447	8.7337	8.7445	8.7661	8.7425	9.1995	9.6555
Cr	4.3550	4.5908	4.5837	4.5905	4.6044	4.5892	4.8288	5.0677
Ta	7.7200	8.1428	8.1360	8.1430	8.1571	8.1422	8.5690	8.9948
Nb	7.1868	7.5710	7.5535	7.5703	7.6040	7.5668	7.9600	8.3518
V	5.5017	5.8010	5.7936	5.8009	5.8154	5.7997	6.1030	6.4054

to the mono-vacancy and di-vacancy, the formation energy of each type of configuration of the tri-vacancy in alkali metals is much lower than that in transition metals. Furthermore, in the five alkali metals, Li corresponds to the highest formation energy, Na, K and Rb are nearly same and Cs is the lowest. In the seven transition metals, the

Table 6 Binding energy (eV) of eight-type configurations of the tri-vacancy in BCC metals.

Metals	$E_{3b}^{[112]}$	$E_{3b}^{[113]}$	$E_{3b}^{[115]}$	$E_{3b}^{[124]}$	$E_{3b}^{[223]}$	$E_{3b}^{[226]}$	$E_{3b}^{[235]}$	$E_{3b}^{[333]}$
Li	0.2053	0.1367	0.1368	0.1366	0.1363	0.1366	0.0679	-0.0007
Na	0.1452	0.0966	0.0968	0.0966	0.0963	0.0966	0.0479	-0.0008
K	0.1454	0.0967	0.0969	0.0967	0.0963	0.0967	0.0479	-0.0008
Rb	0.1460	0.0972	0.0973	0.0972	0.0969	0.0971	0.0483	-0.0005
Cs	0.1385	0.0922	0.0923	0.0921	0.0918	0.0921	0.0457	-0.0007
Fe	0.7665	0.5081	0.5101	0.5079	0.5035	0.5079	0.2483	-0.0110
W	1.6748	1.0999	1.1104	1.0999	1.0788	1.1088	0.5208	-0.0588
Mo	1.2998	0.8486	0.8597	0.8489	0.8272	0.8509	0.3938	-0.0622
Cr	0.6729	0.4370	0.4441	0.4373	0.4234	0.4386	0.1990	-0.0399
Ta	1.2370	0.8142	0.8210	0.8140	0.7999	0.8148	0.3881	-0.0378
Nb	1.0658	0.6816	0.6991	0.6823	0.6486	0.6858	0.2926	-0.0992
V	0.8629	0.5636	0.5709	0.5637	0.5492	0.5649	0.2616	-0.0409

formation energy of each type configuration of the tri-vacancy decreases for W, Mo, Ta, Nb, V, Fe and Cr successively. For each metal, the [112] tri-vacancy constructed by two first- and one second-nearest-neighbor vacancies corresponds to the lowest formation energy, the [113], [115], [124], [223] and [226] tri-vacancies are nearly the same, and the [235] and [333] tri-vacancies are the two highest formation energies. Combining with the formation energies corresponding to three-type configurations of the di-vacancy, we can conclude that the favorable configurations of the multi-vacancy are those composed with the nearest-neighbor vacancies. On the other hand, there is a concentration tendency for the vacancies in BCC metals and maybe the other structured metals. This conclusion is consistent with the experimental results that the voids [20, 21] and crackles [22] are often observed in the materials.

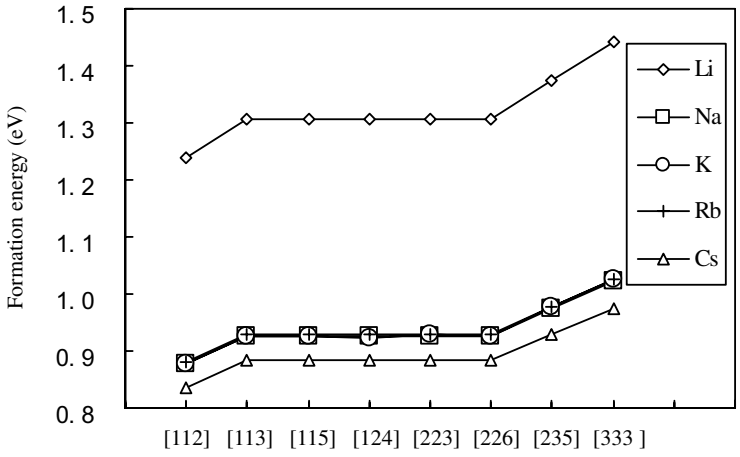

Fig. 3 Formation energy for eight-type configurations of tri-vacancy in BCC alkali metals.

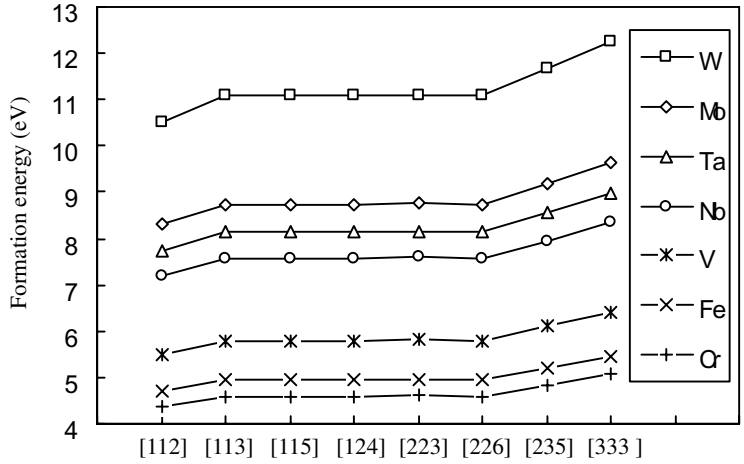

Fig. 4 Formation energy for eight-type configuration of tri-vacancy in BCC transition metals.

The binding energies of eight-type configurations of the tri-vacancy in alkali metals and transition metals are illustrated in Fig. 5 and Fig. 6 respectively. Except for the [333] tri-vacancy which is difficult to form due to its negative binding energy, the binding energy of each type of configuration of the remaining tri-vacancies in the alkali metals is lower than that in transition metals. Furthermore, in the five alkali metals, Li corresponds to the highest binding energy, Na, K and Rb are nearly the same and Cs is the lowest. In the seven transition metals, the binding energy of each type of configuration of the tri-vacancy decreases for W, Mo, Ta, Nb, V, Fe and Cr successively. These are similar to the results of the di-vacancy. For each metal, the [112] tri-vacancy corresponds to the highest binding energy, which shows the [112] tri-vacancy is the most stable. In the remaining formable seven-type configurations of the tri-vacancy, the [113], [115], [124], [223] and [226] tri-vacancies are nearly the same, and the [235] tri-vacancy has the lowest binding energy.

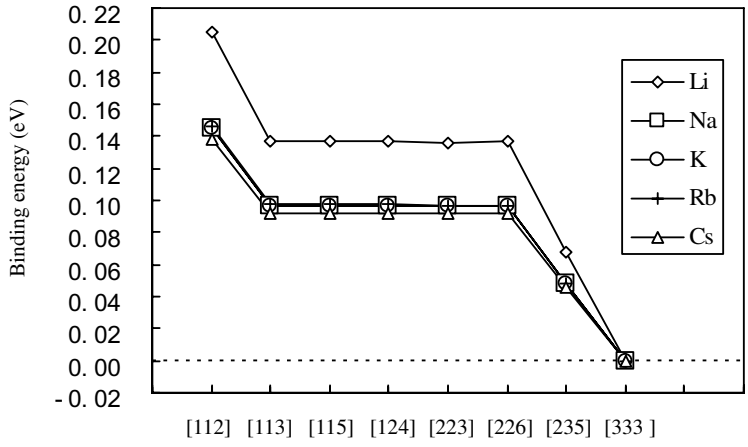

Fig. 5 The binding energy for eight-type configurations of tri-vacancy in BCC alkali metals.

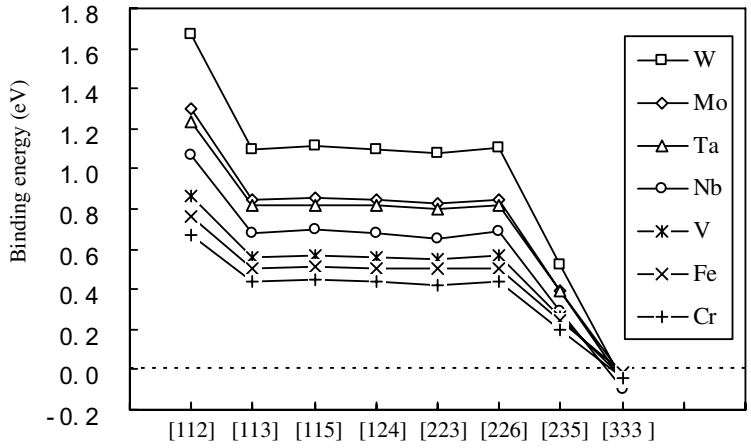

Fig. 6 The binding energy for eight-type configurations of tri-vacancy in BCC transition metals.

In fact, there is a correlation between the atomic number and the formation energy of the mono-, di- and tri- vacancy in the alkali metals and the transition metals. As shown in Fig. 7 and Fig. 8 respectively, the formation energies of the mono-, di- and tri-vacancy decrease with increasing the atomic number of the alkali metals, but increase with increasing the atomic number of the transition metals. Such a correlation also exists between the atomic number and the cohesive energy E_c of the alkali metals and the transition metals and can be explained in view of the cohesive energy. From Eqs. (19) and (21), we know that there is an inverse correlation between the atomic number and the binding energy of the di- and tri- vacancy in the alkali metals and the transition metals.

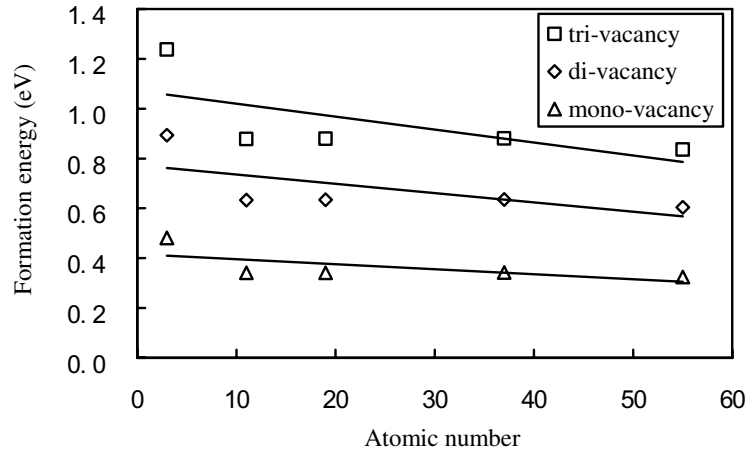

Fig. 7 Correlation between the atomic number and the formation energies of the mono-, di- and tri- vacancy.

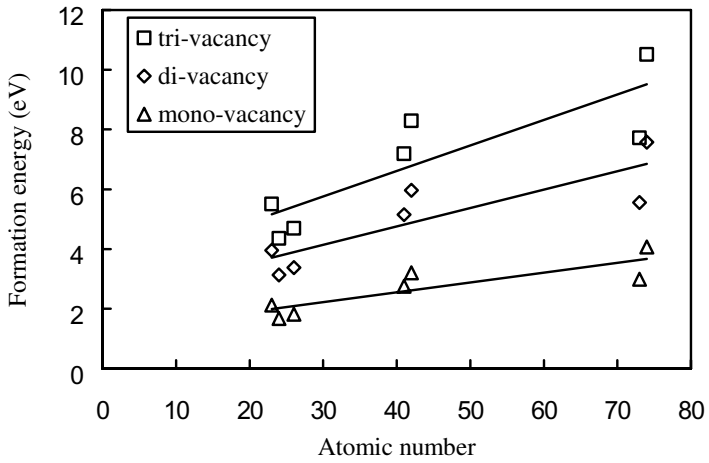

Fig. 8 Correlation between the atomic number and formation energies of the mono-, di- and tri- vacancy in transition metals.

4 Conclusions

The formation energy of the mono-vacancy and both the formation energy and binding energy of three-type configurations of the di-vacancy and eight-type configurations of the tri-vacancy in BCC alkali metals and transition metals have been calculated by using the modified analytical embedded atom method (MAEAM). The following conclusions are obtained.

(1) The formation energies of the mono-vacancy, three-type configurations of the di-vacancy and eight-type configurations of the tri-vacancy in the alkali metals are much lower than that in the transition metals. Furthermore, in the five alkali metals, Li corresponds to the highest formation energy, Na, K and Rb are nearly the same and Cs is the lowest. In seven transition metals, the formation energy decreases for W, Mo, Ta, Nb, V, Fe and Cr successively.

(2) From the minimum of the formation energy or maximum of the binding energy, the favorable configurations of the di-vacancy are the first-nearest-neighbor (FN) and the second-nearest-neighbor (SN), and the favorable configuration of the tri-vacancy is [112] constructed by two first- and one second-nearest-neighbor vacancies. That is the favorable configurations of the multi-vacancy are those composed with the nearest-neighbor vacancies. On the other hand, there is a concentration tendency for the vacancies in BCC metals.

(3) The formation energies of the mono-, di- and tri- vacancy decrease with increasing the atomic number of the alkali metals, but increase with increasing the atomic number of the transition metals.

Acknowledgment

The authors would like to acknowledge the State Key Development Program for Basic Research of China (Grant No. 2004CB619302) and the National Natural Science Foundation of China (Grant No. 50271038) for providing financial support for this research.

References

[1] J.M. Zhang, K.W. Xu and V. Ji: "Competition between surface and strain energy during grain growth in free-standing and attached Ag and Cu films on Si substractes", *Appl. Surf. Sci.*, Vol. 187, (2002), pp. 60–67.

[2] T.R. Mattsson and A.E. Mattsson: "Calculating the vacancy formation energy in metals: Pt, Pd and Mo", *Phys. Rev. B*, Vol. 66, (2002), art. 214110.

[3] K.F. McCarty, J.A. Nobel and N.C. Bartelt: "Vacancies in solids and the stability of surface morphology", *Nature*, Vol. 412, (2001), pp. 622–625.

[4] Y. Kraftmakher: "Equilibrium vacancies and thermophysical properties of metals", *Phys. Rep.*, Vol. 299, (1998), pp. 79–188.

[5] D. Tumball, H.S. Rosenbaum and H.N. Teatfis: "Kinetics of clustering in some Aluminum alloys", *Acta Metall.*, Vol. 8, (1960), pp. 277–295.

[6] A.V. Kozlov and V.V. Kirsanov: "Radiation defect formation and evolution in C0.03Cr20Ni16Mn6 steel under low-temperature neutron irradiation and their effecton physical and mechanual properties of steel", *J. Nucl. Mat.*, Vol. 233–237, (1996), pp. 1062–1066.

[7] R.S. Brusa, W. Deng, G.P. Karwasz and A. Zecca: "Doppler-broadening measurements of positron annihilation with high-momentum electrons in pure elements", *Nucl. Instrum. Meth. B*, Vol. 194, (2002), pp. 519–531.

[8] R.A. Johnson: "Alloy models with the embedded-atom method", *Phys. Rev. B*, Vol. 39, (1989), pp. 12554–12559.

[9] R.A. Johnson and D.J. Oh: "Analytic embedded atom method model for BCC metals", *J. Mat. Res.*, Vol. 4, (1989), pp. 1195–1201.

[10] R.A. Johnson: "Analytic nearest-neighbor model for fcc metals", *Phys. Rev. B*, Vol. 37, (1988), pp. 3924–3931.

[11] W.Y. Hu, B.W. Zhang, X.L. Shu and B.Y. Huang: "Calculation of formation enthalpies and phase stability for Ru-Al alloys using an analytic embedded atom model", *J. Alloy. Compd.*, Vol. 287, (1999), pp. 159–162.

[12] B.W. Zhang, Y.F. Ouyang, S.Z. Liao and Z.P. Jin: "An analytic MEAM model for all BCC transition metals", *Physica B*, Vol. 262, (1999), pp. 218–225.

[13] X.L. Shu, W.Y. Hu, H.N. Xiao and H.Q. Deng: "Vacancies and Antisites in B2 FeAl and DO_3 Fe_3Al with a Modified Analytic EAM Model", *J. Mater. Sci. Technol*, Vol. 17, (2001), pp. 601–604.

[14] J.H. Rose, J.R. Smith, F. Guinea and J. Ferante: "Universal features of the equation of state of metals", *Phys. Rev. B*, Vol. 29, (1984), pp. 2963–2969.

[15] B.W. Zhang, W.Y. Hu and X.L. Shu: "MAEAM theory", In: *Theory of Embedded Atom Method and Its Application to Materials Science – Atomic Scale Materials Design Theory*, Hunan University Press, Changsha, 2003, pp. 245–251 (in Chinese).

[16] M.L. Swanson, G.R. Piercy, G.V. Kidson and A. F. Quenneville: "Defects in quenched zirconium", *J. Nucl. Mat.*, Vol. 34, (1970), pp. 340–342.

[17] K. Maier, M. Peo, B. Saile, H.E. Schaefer and A. Seeger: "High-temperature positron annihilation and vacancy formation in refractory metals", *Philos. Mag. A*, Vol. 40, (1979), pp. 701–728.

[18] Y.F. Ouyang, B.W. Zhang and S.Z. Liao: "Calculation of Self-diffusion Activation Energies for Alkaline Metals With Embedded Atom Method", *Sci. China A*, Vol. 37, (1994), pp. 1232–1240

[19] B.W. Zhang, W.Y. Hu and X.L. Shu (Eds): "Calculation of the point defects and diffusion properties in pure metal elements by using MAEAM theory", In: *Theory of Embedded Atom Method and Its Application to Materials Science-Atomic Scale Materials Design Theory*, Hunan University Press, Changsha, 2003, p. 300 (in Chinese).

[20] R.P. Vinci, T.N. Marieb and J.C. Bravman: "Non-destructive evaluation of strains and voiding in passivated copper metallizations", *Mater. Res. Soc. Symp. Proc.*, Vol. 308, (1993), pp. 297–302.

[21] P. Borgensen, J.K. Lee, R. Gleixner and C.Y. Li: "Thermal-stress-induced voiding in narrow, passivated Cu lines", *Appl. Phys. Lett.*, Vol. 60, (1992), pp. 1706–1708.

[22] J.M. Zhang and K.W. Xu: "Yield strengths and stress induced crackles in copper films: effects of substrate and passivated layer", *Chinese Phys.*, Vol. 13, (2004), pp. 205–211.